IEEE Photonics Journal
An IEEE Photonics Society Publication

Open Access

Vanadium Dioxide-Based Bifunctional Metamaterial for Terahertz Waves

Volume 12, Number 1, February 2020

Man Zhang
Jiahe Zhang
Apeng Chen
Zhengyong Song

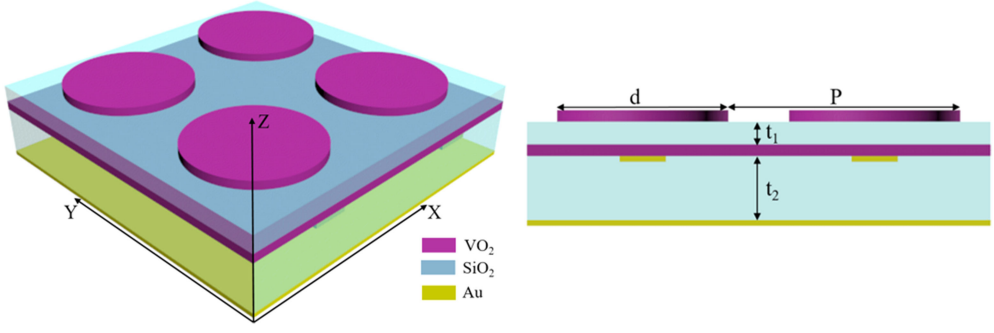

DOI: 10.1109/JPHOT.2019.2958340

IEEE photonics SOCIETY
IEEE

Vanadium Dioxide-Based Bifunctional Metamaterial for Terahertz Waves

Man Zhang, Jiahe Zhang, Apeng Chen, and Zhengyong Song

Institute of Electromagnetics and Acoustics, Xiamen University, Xiamen 361005, China

DOI:10.1109/JPHOT.2019.2958340

Manuscript received November 29, 2019; accepted December 4, 2019. Date of publication December 9, 2019; date of current version January 7, 2020. This work was supported by the National Natural Science Foundation of China (NSFC) under Grants 11974294 and 11504305. Corresponding author: Zhengyong Song (email: zhysong@xmu.edu.cn).

Abstract: A vanadium dioxide-based multilayer metamaterial is proposed with bifunctional properties of absorption and polarization conversion. When vanadium dioxide is in the metallic state, the designed system behaves as a single-band absorber which is composed of a vanadium dioxide disk-shaped array, a silica spacer, and a vanadium dioxide continuous film. The performance of absorption can be tuned by changing either the diameter of disk or the thickness of silica. The design of this absorber is robust against incident polarization and incident angle. The proposed single-band absorber may be generally applied for plasmonic detection, cavity resonator, and optical band-stop filter. When vanadium dioxide is in the insulating state, the designed system behaves as a cross polarization converter which mainly consists of a one-dimensional metallic strip-shaped array, a silica spacer, and a metallic continuous film. The designed metamaterial can convert a linear plane wave into its corresponding cross-polarized wave with the efficiency of $>$90% in the frequency of 2.0-3.0 THz. The physical mechanism of polarization conversion is explained by a simple picture. The proposed metamaterial could be a potential candidate for the modern device of polarization control.

Index Terms: Absorption, metamaterial, polarization, vanadium dioxide.

1. Introduction

In the past decade, metamaterials, artificially manufactured materials arranged in periodic arrays, have attracted considerable research interest of researchers in the fields of electromagnetics and optics. This is because their unique electromagnetic properties and phenomena in many areas cannot be realized in natural materials, including negative refractive index [1]–[3], perfect lens [4]–[6], and polarization converter [7]–[9]. By designing artificial "meta-atoms", the subwavelength structure of metamaterial can be flexibly tuned because it is determined by structures of the internal design rather than the chemical composition. This characteristic enables metamaterial to have designable effective permittivity and permeability. Different kinds of metamaterials have been proposed to meet lots of applications, such as wavefront control [10]–[12] and perfect absorption [13]–[15]. But most of designs are not easily changed once they are fabricated. With the development of metamaterial technology, in order to achieve active tunability and/or reconfigurability, metamaterial can be combined with graphene [16]–[18], phase change material [19]–[23], liquid crystal [24], ferrite [25], diode [26], and structure change [27].

The response of metamaterial can be manipulated by integrating materials with adjustable electro-optic properties. Now, many efforts have been made to develop tunable systems. In view of

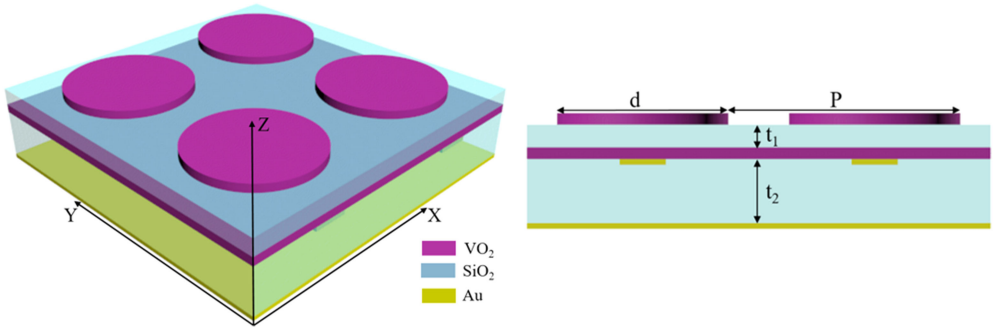

Fig. 1. Three-dimensional schematic of the proposed metamaterial and its side view.

the wide range of potential applications, various phase change materials are studied. Vanadium dioxide (VO_2) undergoes a structural transformation from a monoclinic phase to a tetragonal phase around 340 K [28]–[31]. Phase transition in VO_2 can be caused by external electrical, optical, or thermal excitation. The room temperature of phase transition enables people to employ this characteristic in many different applications. With the occurrence of phase transition, the conductivity of VO_2 varies significantly by 4-5 orders of magnitude, which can control the optical properties of nano-photonic structures. Besides, the reversible change between insulator and metal makes VO_2 attractive for reconfiguration. Therefore, it is a candidate material for electrical and optical applications, such as switch [32], sensor [33], and modulator [34]. In this work, a multilayer metamaterial using phase transition of VO_2 is presented, and it can be switched from a single-band absorber to a cross polarization converter. When VO_2 is in the metallic state, the designed configuration behaves as a perfect single-band absorber based on two-dimensional arrays of VO_2 disk on a VO_2 film. The performance of absorption is polarization-insensitive and angle-independent. When VO_2 is in the insulating state, the designed configuration behaves as an efficient cross polarization converter working in the reflective mode at terahertz frequencies. It can convert a linear-polarized wave to its orthogonal direction. Because of the subwavelength size of the unit cell, the performance of the proposed structure is still good for oblique incidence even up to 45°.

2. Design and Method

Figure 1 shows the schematic of the designed configuration, which consists of six layers. Each layer is listed as follows: VO_2 disks, silica (SiO_2) layer, VO_2 film, metallic strip, SiO_2 layer, and metallic film. Geometric parameters of the structure are given as follows: period $P = 40\ \mu$m, diameter $d = 29.03\ \mu$m, thickness of the top SiO_2 $t_1 = 4.05\ \mu$m, thickness of the bottom SiO_2 $t_2 = 11.0\ \mu$m, and width of the metallic strip 9.5 μm. The thicknesses of VO_2 disk and VO_2 film are 1 μm. The thickness of the metallic strip and film is 0.5 μm. The frequency-dependent complex dielectric permittivity of VO_2 is described by Drude model $\varepsilon(\omega) = \varepsilon_\infty - \frac{\omega_p^2(\sigma)}{\omega^2 + i\gamma\omega}$ in the terahertz range, where $\varepsilon_\infty = 12$ is the dielectric permittivity in the infinite frequency, $\omega_p(\sigma)$ is the plasma frequency dependent on conductivity and γ is the collision frequency [35]–[38]. In addition, $\omega_p^2(\sigma)$ and σ are proportional to free carrier density. The plasma frequency at σ can be approximately defined by $\omega_p^2(\sigma) = \frac{\sigma}{\sigma_0}\omega_p^2(\sigma_0)$ with $\sigma_0 = 3 \times 10^5$ S/m, $\omega_p(\sigma_0) = 1.4 \times 10^{15}$ rad/s, and $\gamma = 5.75 \times 10^{13}$ rad/s which is independent of σ. The phase-transition process of VO_2 is accompanied by great changes in both conductivity and dielectric permittivity. In the calculation process, different permittivities of VO_2 are adopted for different phase states. In our simulation, the conductivity of VO_2 is assumed to be 2×10^5 S/m (0 S/m) for the metallic (insulating) state. The relative dielectric permittivity of the insulating VO_2 is set to 12. These two assumptions can simulate the phase-transition process of VO_2. The conductivity of gold in the terahertz range is considered as 4.561×10^7 S/m. The

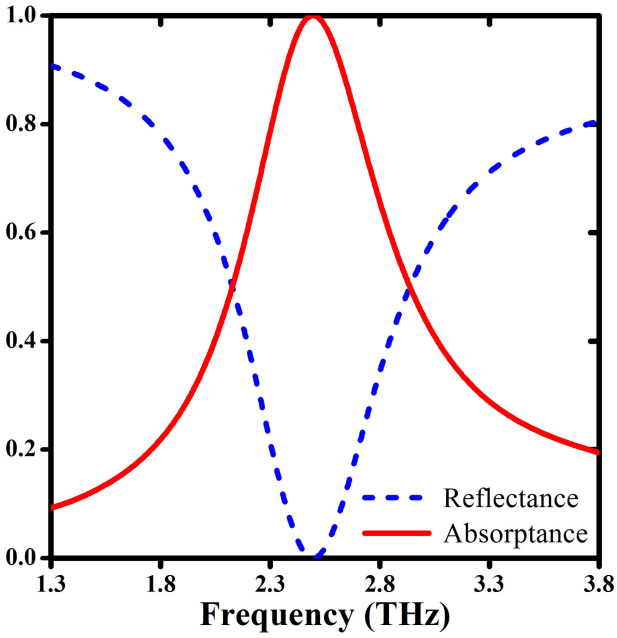

Fig. 2. Simulated reflectance and absorptance under normal incidence.

dielectric permittivity of SiO_2 is set as 3.8 [39], [40]. Three-dimensional finite element method is used in calculation. Unit cell boundary conditions are set in the *x* and *y* directions. In calculation, fine mesh is carefully chosen to ensure the convergence of the result.

3. Results and Discussions

3.1 The Designed Switchable Metamaterial Behaves as a Single-Band Absorber When VO$_2$ Is in the Metallic State

As the thickness (1 μm) of the VO_2 film is thicker than the skin depth to block the wave transmittance (T) in the terahertz region, T of the absorber is nearly zero ($T \approx 0$). Therefore, absorptance ($A = 1 - R - T = 1 - |S_{11}|^2 - |S_{21}|^2$) of the structure is equal to $1 - R$. Figure 2 shows the reflectance and absorptance spectra of metamaterial structure. The peak of absorptance is 100% at the frequency of 2.5 THz at normal incidence.

In order to obtain the ideal absorption, the impedance of the absorber is necessary to match that of the vacuum. As shown in Fig. 2, the central working wavelength of absorption is $\sim$120 μm. The ratio between this wavelength and period is 3. From the perspective of macroscopic electromagnetics based on effective medium theory, it looks acceptable that when VO_2 is in the metallic state, the designed system can be regarded as an isotropic uniform medium with effective optical parameters (dielectric permittivity ε, magnetic permeability μ, refractive index n, impedance z). The S-parameter retrieved method is used to extract the corresponding effective parameters [41]. The calculated effective optical parameters of the VO_2 disk, the middle spacer, and the VO_2 continuous film are shown in Fig. 3. For an individual VO_2 disk and an individual VO_2 continuous film, they are only electrically responsive to electromagnetic wave. The calculated effective electric resonance in Fig. 3(a) is caused by the VO_2 disk at the frequency of 3.54 THz. Because of the near-field coupling between the VO_2 disk and the VO_2 continuous film, the induced electric current flows oppositely along them. As shown in Fig. 3(b), it clearly presents a magnetic resonance at 2.51 THz. The existence of this kind of magnetic resonance ensures that the condition of impedance matching can be well satisfied at a specific frequency. The imaginary part of refractive index in Fig. 3(c) is

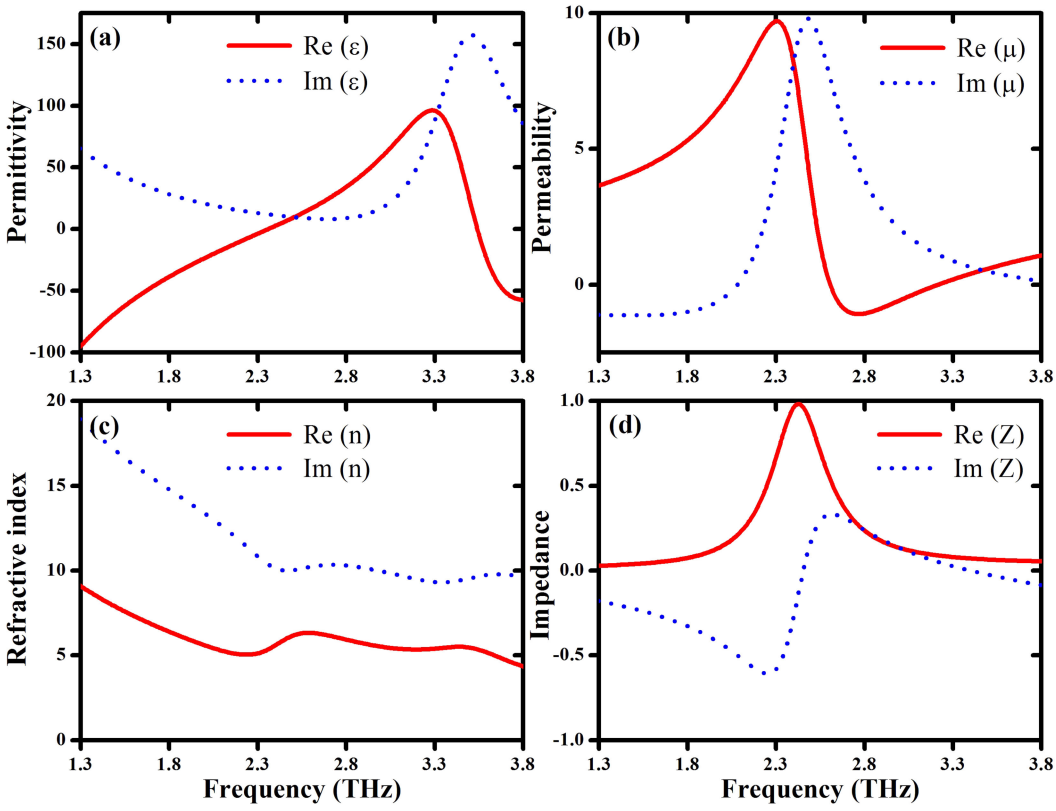

Fig. 3. The retrieved optical parameters (a) permittivity, (b) permeability, (c) refractive index, (d) impedance.

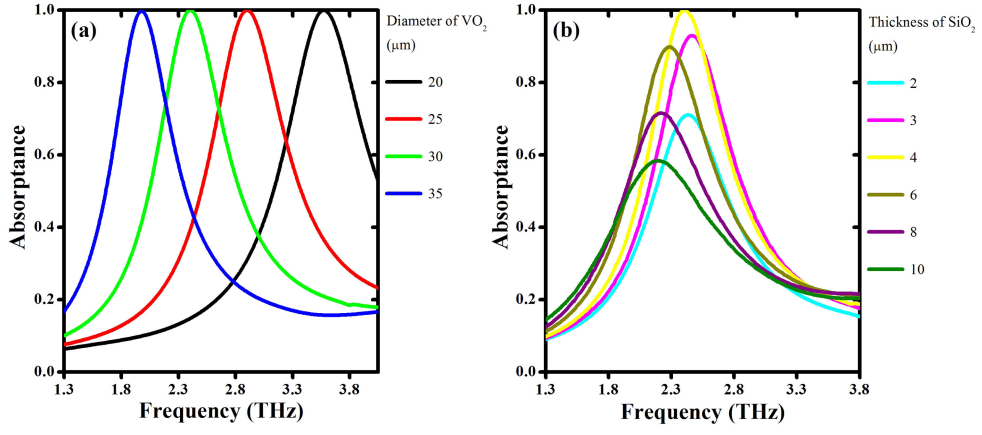

Fig. 4. Calculated absorptance with respect to (a) the diameter and (b) thickness.

enough large, and then it will cause a great attenuation of electromagnetic wave. The real part of the impedance in Fig. 3(d) is close to 1, and the imaginary part is almost zero. As a result, there is a frequency band where reflectance is minimized and absorptance is maximized.

Absorption peak can be tuned by varying the disk diameter and the SiO_2 thickness. Figure 4(a) shows the absorptance spectra for various disk diameters. The increase in the disk diameter results

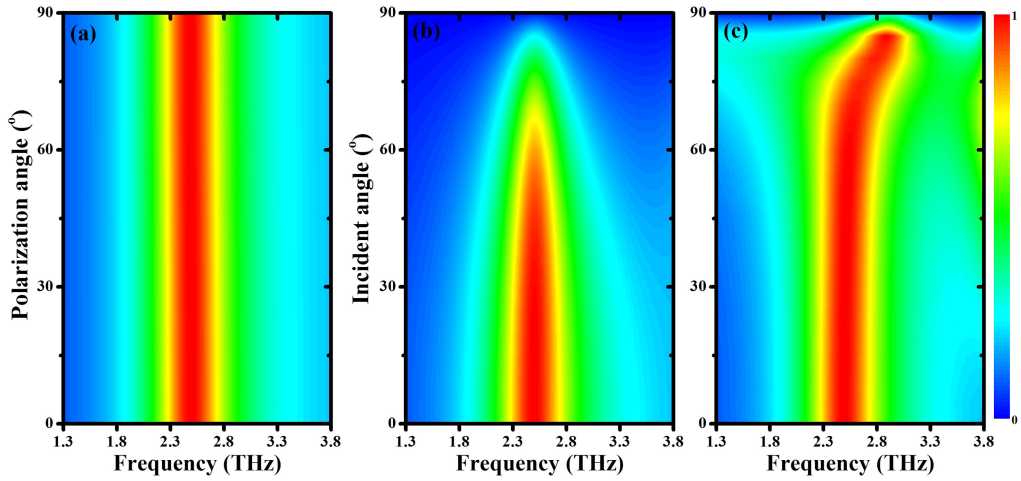

Fig. 5. Simulated absorptance for the proposed absorber at different polarization angles under (a) normal incidence and incident angles for (b) TE and (c) TM polarizations.

in a red shift in the resonant frequency. The intensity remains unchanged. On the other hand, when the thickness of SiO_2 layer increases from 2 μm to 10 μm in Fig. 4(b), the intensity of absorption firstly increases and then decreases and the working position has a little variation. The absorption peak is maximized when the SiO_2 thickness is around 4 μm.

The influences of incident polarization and incident angle on absorptance are investigated. Figure 5(a) shows the absorptance as a function of the variation of polarization angle. The results show that absorptance is completely insensitive to the change of polarization angle under normal incidence. The rotation symmetry of the designed configuration retains polarization-insensitive performance of the system under normal incidence, which is very useful in many applications. Also, it is very important for an absorber to work well at oblique incidence. In order to deeply analyze absorption behavior of this structure, the performance of absorber is studied under oblique incidence. In Fig. 5(b)–(c), as the incident angle increases from 0° to 90°, absorptances of transverse electric (TE)-polarized and transverse magnetic (TM)-polarized waves are shown as a function of incident angle and frequency. Red region means high absorptance. Absorptance of TE-polarized wave in Fig. 5(b) is stable within the incident angle of 45°. When incident angle is larger than 45°, intensity of absorptance decreases and bandwidth becomes narrower. It is mainly caused by the decrease of parallel component of magnetic field with the increase of incident angle. Absorptance of TM-polarized wave in Fig. 5(c) can reach 100% at the resonant frequency for the incident angle from 0° to 75°. This is because magnetic field of TM-polarized wave is always parallel to the xoy plane. This angle-insensitive performance is a result of strong coupling of localized surface plasmon with incident wave.

3.2 The Designed Switchable Metamaterial Behaves as a Cross Polarization Converter When VO$_2$ Is in the Insulating State

When the incident wave is polarized along the polarization angle 45°, the simulated result of cross-polarization reflectance is shown in Fig. 6(a). As shown in Fig. 6(a), the peak of polarization conversion occurs with the efficiency of $>$90% in the frequency of 2.0-3.0 THz. Therefore, at this frequency range, the incident wave shows almost perfect orthogonal polarization conversion. The working mechanism can be simply explained by the following analysis. The electric field (E_i) of incident electromagnetic wave along the polarization angle 45° can be decomposed into two vertical components, E_{ix} and E_{iy}. Generally, the field of reflection is composed of x and y

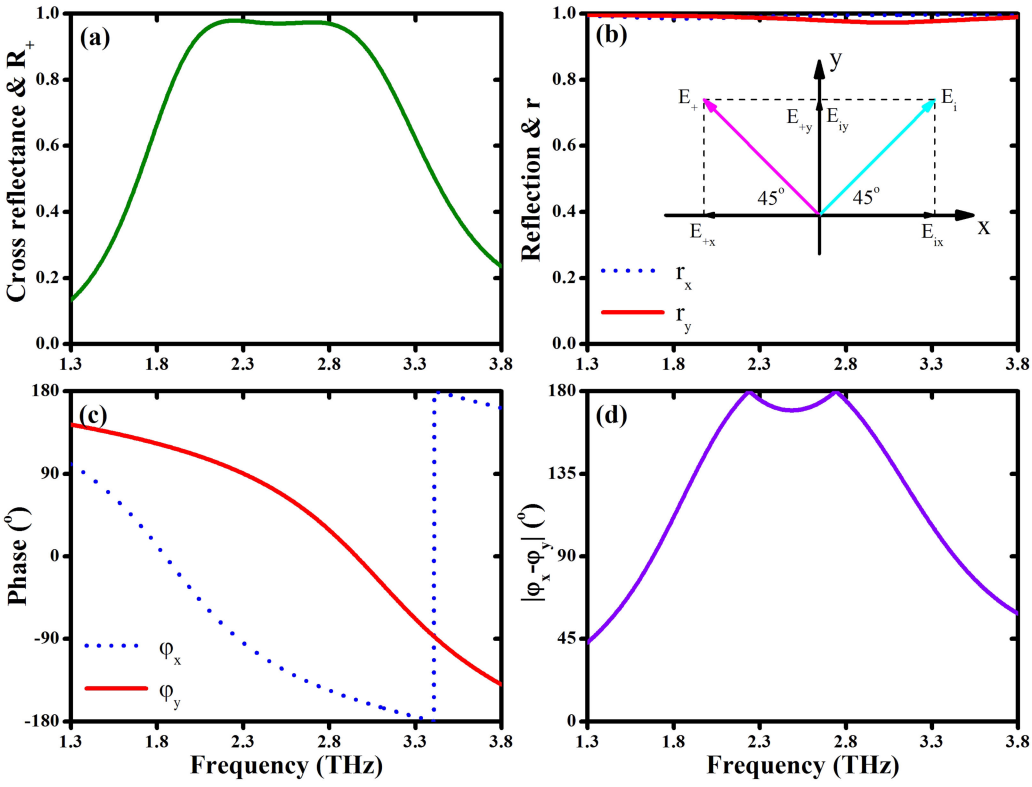

Fig. 6. (a) Reflectance of cross-polarized wave. (b) Reflection amplitudes and (c) phases for x and y-polarized waves. (d) Reflection phase difference between x and y directions. Inset in (b) means that incident electric field is decomposed into two orthogonal components along the x- and y-axes and reflected electric field is rotated by 90°.

components. Due to the existence of anisotropy of the designed structure, the reflected wave along the x and y axis has different reflection amplitude and phase. Understanding this point, the proposed design is analyzed, and the amplitude and phase of reflection coefficient are studied. The amplitude and phase of the reflection coefficients along x and y directions are shown in Fig. 6(b)–(c). When the amplitudes of E_{+x} and E_{+y} is nearly equal and the phase difference in Fig. 6(d) between them is ∼180°, the polarization direction of the reflected wave will be orthogonal to that of the incident wave and then cross polarization conversion is realized.

Parametric analyses are conducted to study the influences of strip width and SiO_2 thickness on the performance. Figure 7(a) shows the effect of changing the width of gold strip on the cross-polarized reflectance. When the width increases from 4 μm to 9.5 μm, cross-polarization reflectance has one peak and the intensity gradiently increases. For smaller strip width, the bandwidth is small. When the width increases from 9.5 μm to 20 μm, cross-polarization reflectance has two peaks and the intensity between two peaks gradiently decreases. The optimum width is 9.5 μm. The influence of the thickness of SiO_2 is also studied. The results are shown in Fig. 7(b). With the increase of thickness, the peak of cross-polarization reflectance shifts red. When the thickness is smaller, there is one peak. When the thickness is larger than 11 μm, there are two peaks. So cross-polarization reflectance is sensitive to the thickness of SiO_2.

The effects of polarization and incident angle are also studied. The result in Fig. 8(a) is cross-polarization reflectance as a function of polarization angle and frequency under normal incidence. When the polarization angle is 0° or 90°, the value of cross-polarization reflectance is nearly zero. This result is very reasonable, because E and H fields of incident wave are parallel to the coordinate

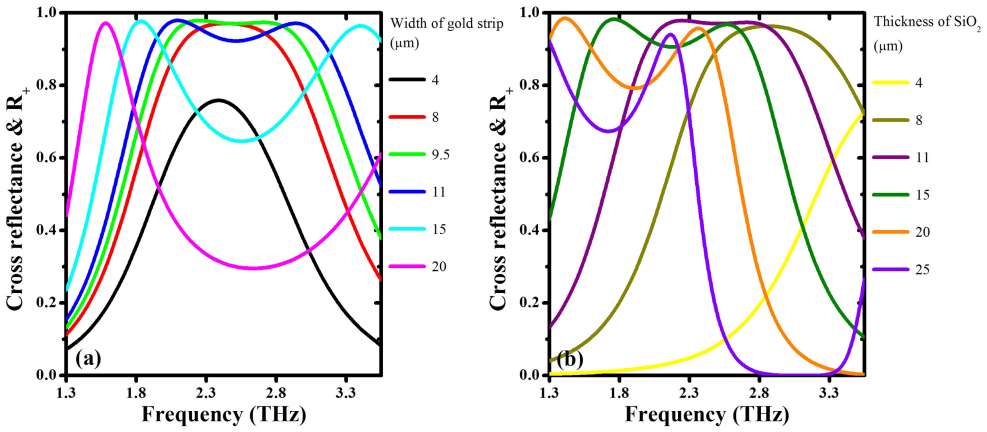

Fig. 7. Variation of cross-polarized reflectance with the variation of (a) the width and (b) the thickness.

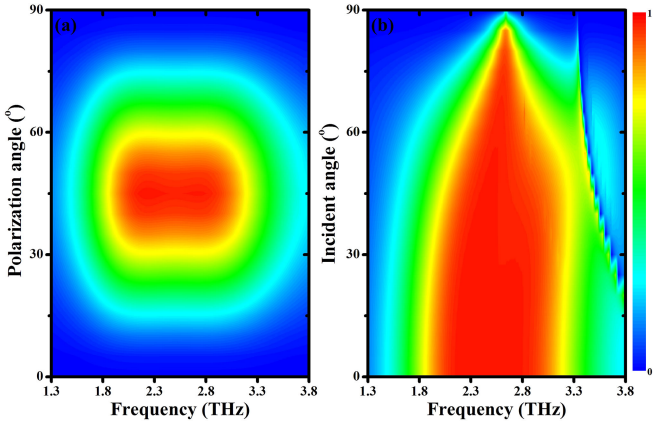

Fig. 8. Reflectance of cross-polarized wave as a function of (a) polarization angle and frequency under normal incidence and (b) incident angle and frequency.

axis and electromagnetic wave cannot feel the existence of anisotropy of the structure. Anisotropy can help to provide different electromagnetic response to incident electric field. When polarization angle is not 0° or 90°, the non-zero value of cross-polarization reflectance can be obtained. Moreover, reflectance of polarization conversion has the highest value when polarization angle is 45°. So structural anisotropy along the x-axis and y-axis plays an important role in the process of design. In order to make the designed polarization converter valuable in many applications, the performance of polarization converter should be stable with the change of incident angle. As shown in Fig. 8(b), the intensity and bandwidth of cross-polarization reflectance is quite stable for the change of incident angle until 45°. Because the ratio of wavelength 100 μm (3.0 THz) to period 40 μm is $\sim$ 2.5, cross-polarization reflectance can effectively avoid scattering lobes in the working region. When incident angle is larger than 45°, the bandwidth of cross-polarization reflectance will become narrower, and finally converge into a single frequency. So the insensitivity of incident angle within 45° makes the proposed metamaterial candidate for many potential applications.

4. Conclusion

To summarize, a bifunctional metamaterial is designed, and it can be switched from an absorber to a cross polarization converter. When VO$_2$ is in the metallic state, the VO$_2$ disk, the dielectric spacer,

and the VO_2 film will form an efficient single-band absorber in the terahertz frequency [42]–[45]. By properly designing structure, this absorber work very well for TE and TM polarizations even at the incident angle 45°. The designed absorber may have potential applications in sensing, detection, and filtering for terahertz wave. When VO_2 is in the insulating state, the designed system behaves as a highly-efficient reflective polarization converter in the terahertz frequency. The efficiency of cross polarization is $>$90% from 2.0 THz to 3.0 THz under normal incidence. It also shows excellent performance for oblique incidence.

References

[1] J. B. Pendry, "Negative refraction," *Contemp. Phys.*, vol. 45, no. 3, pp. 191–202, 2004.
[2] S. A. Ramakrishna, "Physics of negative refractive index materials," *Rep. Prog. Phys.*, vol. 68, no. 2, pp. 449–521, 2005.
[3] J. F. Zhou, Th. Koschny, L. Zhang, G. Tuttle, and C. M. Soukoulis, "Experimental demonstration of negative index of refraction," *Appl. Phys. Lett.*, vol. 88, no. 22, 2006, Art. no. 221103.
[4] D. R. Smith, D. Schurig, M. Rosenbluth, S. Schultz, S. A. Ramakrishna, and J. B. Pendry, "Limitations on subdiffraction imaging with a negative refractive index slab," *Appl. Phys. Lett.*, vol. 82, no. 10, pp. 1506–1508, 2003.
[5] X. S. Rao and C. K. Ong, "Amplification of evanescent waves in a lossy left-handed material slab," *Phys. Rev. B*, vol. 68, no. 11, 2003, Art. no. 113103.
[6] S. A. Cummer, "Simulated causal subwavelength focusing by a negative refractive index slab," *Appl. Phys. Lett.*, vol. 82, no. 10, pp. 1503–1505, 2003.
[7] J. M. Hao *et al.*, "Manipulating electromagnetic wave polarizations by anisotropic metamaterials," *Phys. Rev. Lett.*, vol. 99, no. 6, 2007, Art. no. 063908.
[8] J. K. Gansel *et al.*, "Gold helix photonic metamaterial as broadband circular polarizer," *Science*, vol. 325, no. 5947, pp. 1513–1515, 2009.
[9] L. Cong *et al.*, "A perfect metamaterial polarization rotator," *Appl. Phys. Lett.*, vol. 103, no. 17, 2013, Art. no. 171107.
[10] N. F. Yu *et al.*, "Light propagation with phase discontinuities: Generalized laws of reflection and refraction," *Science*, vol. 334, no. 6054, pp. 333–337, 2011.
[11] S. L. Sun, Q. He, S. Y. Xiao, Q. Xu, X. Li, and L. Zhou, "Gradient-index meta-surfaces as a bridge linking propagating waves and surface waves," *Nat. Mater.*, vol. 11, no. 5, pp. 426–431, 2012.
[12] T. J. Cui, S. Liu, and L. L. Li, "Information entropy of coding metasurface," *Light-Sci. Appl.*, vol. 5, 2016, Art. no. e16172.
[13] N. I. Landy, S. Sajuyigbe, J. J. Mock, D. R. Smith, and W. J. Padilla, "Perfect metamaterial absorber," *Phys. Rev. Lett.*, vol. 100, no. 20, 2008, Art. no. 207402.
[14] Z. Song, Z. Wang, and M. Wei, "Broadband tunable absorber for terahertz waves based on isotropic silicon metasurfaces," *Mater. Lett.*, vol. 234, pp. 138–141, 2019.
[15] J. M. Hao, J. Wang, X. L. Liu, W. J. Padilla, L. Zhou, and M. Qiu, "High performance optical absorber based on a plasmonic metamaterial," *Appl. Phys. Lett.*, vol. 96, no. 25, 2010, Art. no. 251104.
[16] A. H. Castro Neto, F. Guinea, N. M. R. Peres, K. S. Novoselov, and A. K. Geim, "The electronic properties of graphene," *Rev. Mod. Phys.*, vol. 81, no. 1, pp. 109–162, 2009.
[17] A. Vakil and N. Engheta, "Transformation optics using graphene," *Science*, vol. 332, no. 6035, pp. 1291–1294, 2011.
[18] M. Jablan, H. Buljan, and M. Soljacic, "Plasmonics in graphene at infrared frequencies," *Phys. Rev. B*, vol. 80, no. 24, 2009, Art. no. 245435.
[19] A. K. U. Michel, P. Zalden, D. N. Chigrin, M. Wuttig, A. M. Lindenberg, and T. Taubner, "Reversible optical switching of infrared antenna resonances with ultrathin phase-change layers using femtosecond laser pulses," *ACS Photon.*, vol. 1, no. 9, pp. 833–839, 2014.
[20] F. F. Schlich, P. Zalden, A. M. Lindenberg, and R. Spolenak, "Color switching with enhanced optical contrast in ultrathin phase-change materials and semiconductors induced by femtosecond laser pulses," *ACS Photon.*, vol. 2, no. 2, pp. 178–182, 2015.
[21] P. N. Li *et al.*, "Reversible optical switching of highly confined phonon-polaritons with an ultrathin phase-change material," *Nature Mater.*, vol. 15, no. 8, pp. 870–875, 2016.
[22] M. Wei, Z. Song, Y. Deng, Y. Liu, and Q. Chen, "Large-angle mid-infrared absorption switch enabled by polarization-independent GST metasurfaces," *Mater. Lett.*, vol. 236, pp. 350–353, 2019.
[23] Y. Qu *et al.*, "Thermal camouflage based on the phase-changing material GST," *Light-Sci. Appl.*, vol. 7, 2018, Art. no. 26.
[24] T. L. Ting, "Technology of liquid crystal based antenna," *Opt. Exp.*, vol. 27, no. 12, pp. 17138–17153, 2019.
[25] T. Ueda, K. Okamoto, and T. Itoh, "Enhancement of phase-shifting nonreciprocity in metamaterial lines with comb-shaped capacitive stubs on the normally magnetized ferrite substrate," *IEEE Trans. Magn.*, vol. 54, no. 11, Nov. 2018, Art. no. 2502205.
[26] W. Ma, D. L. Jia, Y. Z. Wen, X. M. Yu, Y. Feng, and Y. J. Zhao, "Diode-based microbolometer with performance enhanced by broadband metamaterial absorber," *Opt. Lett.*, vol. 41, no. 13, pp. 2974–2977, 2016.
[27] A. Rafsanjani and D. Pasini, "Bistable auxetic mechanical metamaterials inspired by ancient geometric motifs," *Extreme Mech. Lett.*, vol. 9, pp. 291–296, 2016.
[28] T. Driscoll *et al.*, "Memory metamaterials," *Science*, vol. 325, no. 5947, pp. 1518–1521, 2009.
[29] Y. G. Jeong *et al.*, "A vanadium dioxide metamaterial disengaged from insulator-to-metal transition," *Nano Lett.*, vol. 15, no. 10, pp. 6318–6323, 2015.

[30] L. Liu, L. Kang, T. S. Mayer, and D. H. Werner, "Hybrid metamaterials for electrically triggered multifunctional control," *Nature Commun.*, vol. 7, p. 13236, 2016.
[31] G. Zhang, H. Ma, C. Lan, R. Gao, and J. Zhou, "Microwave tunable metamaterial based on semiconductor-to-metal phase transition," *Sci. Rep.*, vol. 7, 2017, Art. no. 5773.
[32] W. Huang, X. Yin, C. Huang, Q. Wang, T. Miao, and Y. Zhu, "Optical switching of a metamaterial by temperature controlling," *Appl. Phys. Lett.*, vol. 96, no. 26, 2010, Art. no. 261908.
[33] H. K. Kim, D. Lee, and S. Lim, "A fluidically tunable metasurface absorber for flexible large-scale wireless ethanol sensor applications," *Sensors*, vol. 16, no. 8, 2016, Art. no. 1246.
[34] H. Cai *et al.*, "Multifunctional hybrid metasurfaces for dynamic tuning of terahertz waves," *Adv. Opt. Mater.*, vol. 6, no. 14, 2018, Art. no. 1800257.
[35] M. Liu *et al.*, "Terahertz-field-induced insulator-to-metal transition in vanadium dioxide metamaterial," *Nature*, vol. 487, no. 7407, pp. 345–348, 2012.
[36] Q. Chu, Z. Song, and Q. H. Liu, "Omnidirectional tunable terahertz analog of electromagnetically induced transparency realized by isotropic vanadium dioxide metasurfaces," *Appl. Phys. Exp.*, vol. 11, no. 8, 2018, Art. no. 082203.
[37] S. Wang, L. Kang, and D. H. Werner, "Hybrid resonators and highly tunable terahertz metamaterials enabled by vanadium dioxide (VO_2)," *Sci. Rep.*, vol. 7, 2017, Art. no. 4326.
[38] Z. Song, Y. Deng, Y. Zhou, and Z. Liu, "Terahertz toroidal metamaterial with tunable properties," *Opt. Exp.*, vol. 27, no. 4, pp. 5792–5797, 2019.
[39] M. Naftaly and R. E. Miles, "Terahertz time-domain spectroscopy of silicate glasses and the relationship to material properties," *J. Appl. Phys.*, vol. 102, no. 4, 2007, Art. no. 043517.
[40] Z. Song, M. Wei, Z. Wang, G. Cai, Y. Liu, and Y. Zhou, "Terahertz absorber with reconfigurable bandwidth based on isotropic vanadium dioxide metasurfaces," *IEEE Photon. J.*, vol. 11, no. 2, Apr. 2019, Art no. 4600607.
[41] D. R. Smith, S. Schultz, P. Markos, and C. M. Soukoulis, "Determination of effective permittivity and permeability of metamaterials from reflection and transmission coefficients," *Phys. Rev. B*, vol. 65, no. 19, 2002, Art. no. 195104.
[42] W. Zhu *et al.*, "Wideband visible-light absorption in an ultrathin silicon nanostructure," *Opt. Exp.*, vol. 25, no. 5, pp. 5781–5786, 2017.
[43] W. Zhu *et al.*, "Multiband coherent perfect absorption in a water-based metasurface," *Opt. Exp.*, vol. 25, no. 14, pp. 15737–15745, 2017.
[44] J. Xie *et al.*, "Water metamaterial for ultra-broadband and wide-angle absorption," *Opt. Exp.*, vol. 26, no. 4, pp. 5052–5059, 2018.
[45] J. Xie *et al.*, "Truly all-dielectric ultra-broadband metamaterial absorber: Water-based and ground-free," *IEEE Antenn. Wirel. Propag. Lett.*, vol. 18, no. 3, pp. 536–540, Mar. 2019.